NEON AOP Surveys of City of Boulder Pre and Post 2013 Flood Event

Tristan Goulden[a], Thomas U. Kampe[a]

[a]National Ecological Observatory Network, 1685 38th St., Suite 100, Boulder, CO 0301

ABSTRACT

The National Ecological Observatory Network (NEON) operates an airborne remote sensing payload which contains a LiDAR (Light Detection and Ranging) sensor (*Kampe et al.*, 2010). LiDAR provides a highly accurate and dense sampling of the earth's surface, enabling a detailed mapping of the land surface topography. Two months prior to a major flood event in Colorado, which occurred in September of 2013, NEON undertook a LIDAR survey of the city of Boulder. Following the flood event, a second LiDAR acquisition was undertaken. A high resolution digital topographic map of the ground surface, termed a DTM (Digital Terrain Model), was produced for each survey at 1 m resolution. The DTMs were subtracted to produce a DTM of difference (DOD) map of the vertical topographic change caused by the flood event. An error analysis of the resulting DTMs generally indicates that changes observed above ±0.1 m are likely due to physical processes related to the flood, while changes below this threshold can be attributed to sensor and processing uncertainty. Resulting topographic changes due to overland flow were detectable in some stream headwater locations, while topographic changes within stream channels were prevalent. Some stream channels exhibited substantial degradation, especially in high slope regions as channels descended through mountainous regions of the landscape. Stream channels also experienced substantial degradation (> 3 m) as the channels transitioned from high to low slopes. Areas of substantial channel deposition were noted within the urban boundary of the City of Boulder. The LIDAR data described in this document is available for public retrieval through request to NEON.

Keywords: Boulder flood, LiDAR, topographic change, erosion

1. INTRODUCTION

Between September 9th 2013 and September 16th 2013, areas of Boulder County experienced an unprecedented storm event which exceeded the 1000 year recurrence interval (*Lukas*, 2013). Within the time period, over 18 inches of rain was observed at the Boulder 3.3 SE rain gauge located in South Boulder (NOAA, 2013). This seven day rainfall total is greater than the average yearly rainfall. The storm event resulted in four deaths, the destruction of 345 homes, and damage estimated to be between 100 and 150 million USD (*Brennan and Aguilar*, 2013). On June 26th and 27th, 2013 the National Ecological Observatory Network (NEON), conducted a LiDAR (Light Detection and Ranging) survey of the city of Boulder as part of an annual engineering test-flight campaign, hereafter referred as the 'pre-flood' acquisition. After the storm event, on October 8th, 2013 NEON conducted a second LiDAR flight of the same area, hereafter referred as the 'post-flood' acquisition. The temporal proximity of the pre-flood and post-flood acquisitions presents an extraordinary opportunity for investigating topographic changes which were driven by the storm event. Furthermore, observed topographic changes can be used for analysis and simulation of future flooding conditions and to update areas of high potential flood risk.

The purpose of this document is to provide information about the procedures used in processing the LIDAR data to determine a map of topographic change, as well as to estimate the quality of the data so users can properly interpret change results. The document will describe the flight acquisition parameters of the pre-flood and post flood surveys, the processing methodology used to create a change detection map, as well as the results of an error analysis. Some guidelines will be offered on how to interpret the results of the change detection in consideration with the associated error analysis. Following this, a description of how to access the data will be provided. This document does not provide the general theoretical background details of LiDAR surveys, which may be necessary for understanding all content. For further information in the theoretical background on LIDAR, readers are referred to *Wehr and Lohr* (1999), *Baltsavias* (1999), *Toth and Shen* (2008), and *Vosselman and Maas* (2010), the airborne remote sensing page of the NEON website (http://www.neoninc.org/science-design/collection-methods/airborne-remote-sensing), and a NEON educational video on LIDAR located at (https://www.youtube.com/user/NEONBetaEDU).

2. LIDAR DATA ACQUISITIONS PARAMETERS

The pre-flood and post-flood surveys were acquired with an Optech Gemini LiDAR sensor (*Optech*, 2008), with serial number 11SEN287, mounted in a Twin Otter aircraft. The pre-flood acquisition occurred on June 26th and June 27th, 2013. The pre-flood surveyed area is approximately bounded at western extents of 105°19'19" W, eastern extent of 105°08'45" W, northern extent of 40°06'01" N and southern extent of 39°57'30" N (Figure 1). Table 1 summarizes the flight parameters that were used during the pre-flood and post-flood acquisitions. The selected parameters for the pre-flood survey resulted in an average point spacing of 3.0 pts/m^2 and an average spacing between adjacent points of 0.58 m. In total, over 703 million point observations were acquired. The post-flood acquisition occurred on Oct. 8th, 2013 and extended further west than the pre-flood acquisition (Figure 1). The post-flood survey area is approximately bounded at a western extent of 105°20'11" W, eastern extent of 105°08'42" W, northern extent of 40°05'50" N and southern extent of 39°57'25" N (Figure 1). The selected survey parameters for the post-flight survey resulted in an average point density of 2.88 pts/m^2 and an average spacing between adjacent points of 0.59 m, with over 729 million points acquired across the survey area.

Table 1 – LiDAR survey parameters for the pre-flood and post-flood acquisitions

Parameter	Pre-flood survey	Post-flood survey
Mean flight altitude	~1500 m a.g.l. (above ground level)	~1800 m a.g.l. (above ground level)
Pulse repetition frequency (PRF)	70 kHz	70 kHz
Scan frequency	33 Hz	33 Hz
Beam divergence (1/e)	0.8 mRad	0.8 mRad
Half scan angle	18°	18°

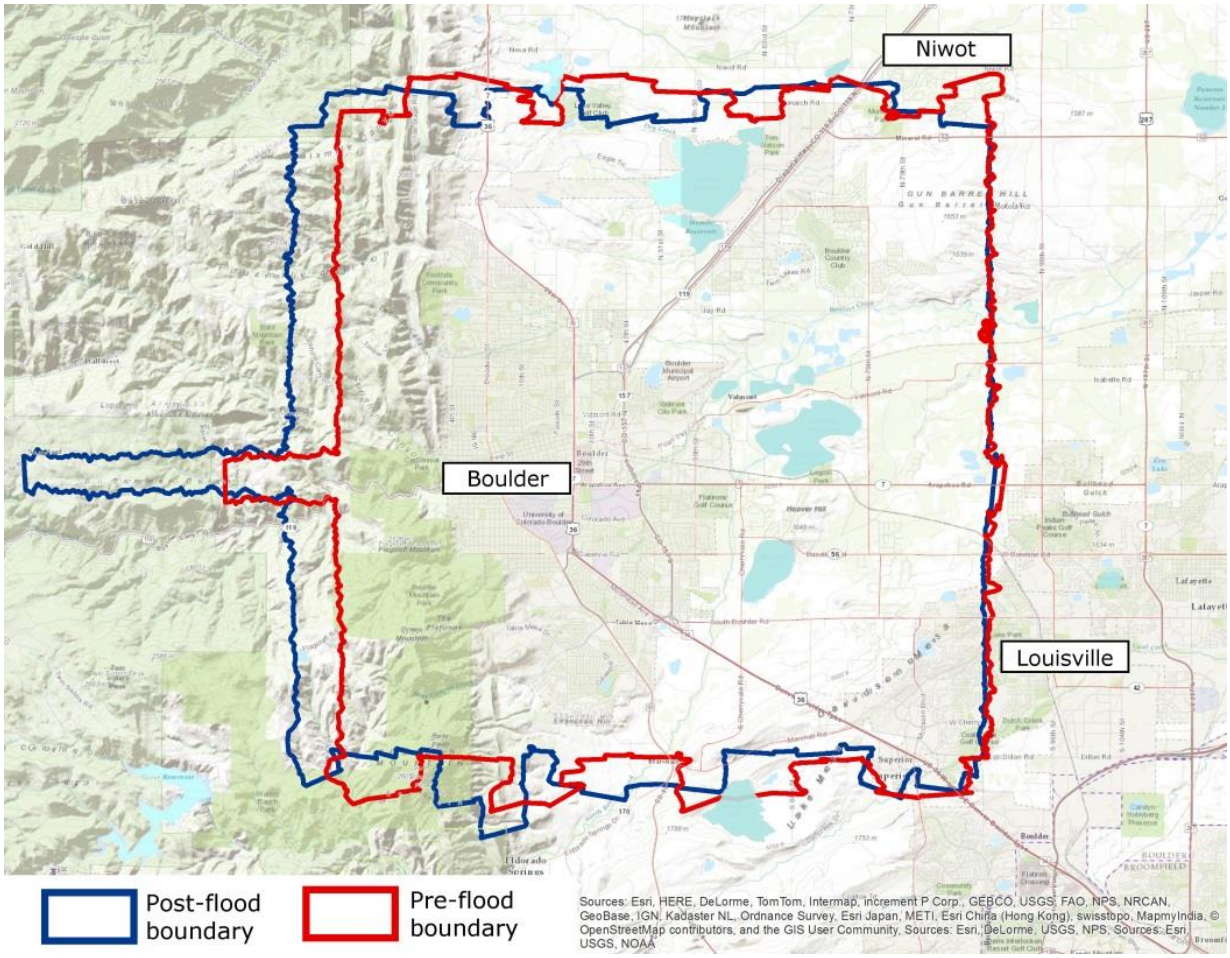

Figure 1 – Boundaries of the pre-flood acquisition and the post-flood acquisition

3. DATA PROCESSING METHODS

3.1 Aircraft trajectory processing

During the pre-flood and post-flood acquisitions, a dual phase (L1/L2) Global Navigation Satellite System (GNSS) receiver was mounted on the roof of the airborne platform to provide absolute aircraft position in the WGS84 datum. A second static global positioning satellite (GPS) receiver was deployed at NEON headquarters (HQ) for the duration of each flight to provide data necessary for differential correction of the aircraft positions. The receiver on the aircraft and at NEON headquarters were set to log GPS signals at 1 second intervals (1 Hz). The position of the basestation at NEON headquarters was determined through the Online Positioning User Service (OPUS) (http://www.ngs.noaa.gov/OPUS/about.jsp), a differential correction

service provided by NOAA. The aircraft position was differentially corrected with respect to the basestation operated at NEON HQ and with locally operating CORS (Continually Operating Reference System) and UNAVCO (University Navstar Consortium) stations. Absolute GPS positions from the airborne GPS receiver were supplemented with observations from an on-board IMU (Inertial Measurement Unit) in a tightly coupled positioning algorithm within Applanix's Paspac MMS 6.2 (*Applanix*, 2013) software to determine the aircraft position every 0.005 s (200 Hz).

3.2 Production of LiDAR point clouds

Georeferencing of the LiDAR point cloud was performed in Optech's LMS software. LMS combines the aircraft trajectory with observed laser ranges, scan angles and calibration information (eccentricity distances, boresight angles), to produce a 'point cloud' of three-dimensional coordinate observations from surface features intercepted by the laser pulses. The point-cloud was produced with horizontal reference to the WGS-84 datum and Universal Transverse Mercator (UTM) mapping frame, and vertical reference to Geoid12A, both in units of meters. Final LIDAR point coordinates are output as LAS 1.3 files. Details of the LAS 1.3 file type can be found in *ASPRS* (2010).

Within LMS, an option to improve the spatial compatibility between adjacent flight lines is available, termed 'refined processing' (*Lindenthal et al.*, 2011). The refined processing algorithm creates planar surfaces from the LiDAR observations of a 'reference' flight line, and matches individual points in an overlapping portion of a 'target' flight line to the planar surfaces in the reference line. A residual offset is determined between a point and its corresponding plane, and used in a least squares adjustment to determine corrective translations and angular shifts between adjacent flight lines. The least squares adjustment results determine the translations and angular shifts which provide the minimum sum of squares of the distance from the points in the target line to the planes in the reference line, providing the optimal compatibility between adjacent strips. In the typical NEON workflow, the refined processing would be applied to both pre-flood and post-flood surveys independently. However, since the primary objective of the pre-flood and post-flood data is to highlight relative differences in topography, all lines from both surveys were simultaneously adjusted with the refined processing routine.

3.3 Production of DTMs

A LiDAR point cloud consists of individual point observations which intercept the terrain in a pseudo-random pattern dependent on the selected survey acquisition parameters. For terrain analysis applications, such as determining topographic changes between surveys, it is desirable to create a continuous terrain surface. The continuous terrain surface is termed a Digital Terrain Model (DTM). Although several forms of DTMs exist, the most common is a regularly spaced grid of cells, each representing a surface elevation (*Moore et al.*, 1993). The grid based DTM facilitates differencing between the pre-flood and post-flood surveys because grid cells from each DTM can be located in the same spatial position and directly subtracted. DTMs for the pre-flood and post-flood surveys were created in the LAStools (http://rapidlasso.com/lastools/) software package. LAStools uses a TIN (Triangular Irregular Network) algorithm for DTM creation. The TIN algorithm connects each LIDAR coordinate observation through a series of contiguous triangular facets. Edges of triangular facets form linear connections between adjacent coordinate observations in the LiDAR point cloud, forming a continuous surface. The TIN algorithm is constrained by the condition that no point can lay within the boundary of a triangular facet. The grid-based DTM is determined by overlaying a regular grid onto the TIN surface and extracting the elevation of each grid node location from the corresponding triangular plane. The DTM grid was established at a 1 m spacing, which was selected based on the ground spacing of the LIDAR point observations of approximately 0.5 m between adjacent points. DTMs created from LIDAR data using TIN surfaces can appear noisy due to the imprecision of individual LIDAR points. To reduce the noise in the grid based DTM, a 3 x 3 moving boxcar averaging filter was applied to the pre-flood and post-flood DTMs. Since our primary interest is in the topographic changes due to the flood, LiDAR returns from surface features such as vegetation are undesirable. Therefore, prior to creation of the DTMs, all LIDAR echoes from surface features have to be identified and removed (Figure 2). LAStools was also used to filter the non-ground LIDAR returns from ground returns. Although the LAStools literature does not identify the exact algorithm in place for filtering ground point, an example of a commonly used ground filtering routine can be seen in *Axelsson* (2000).

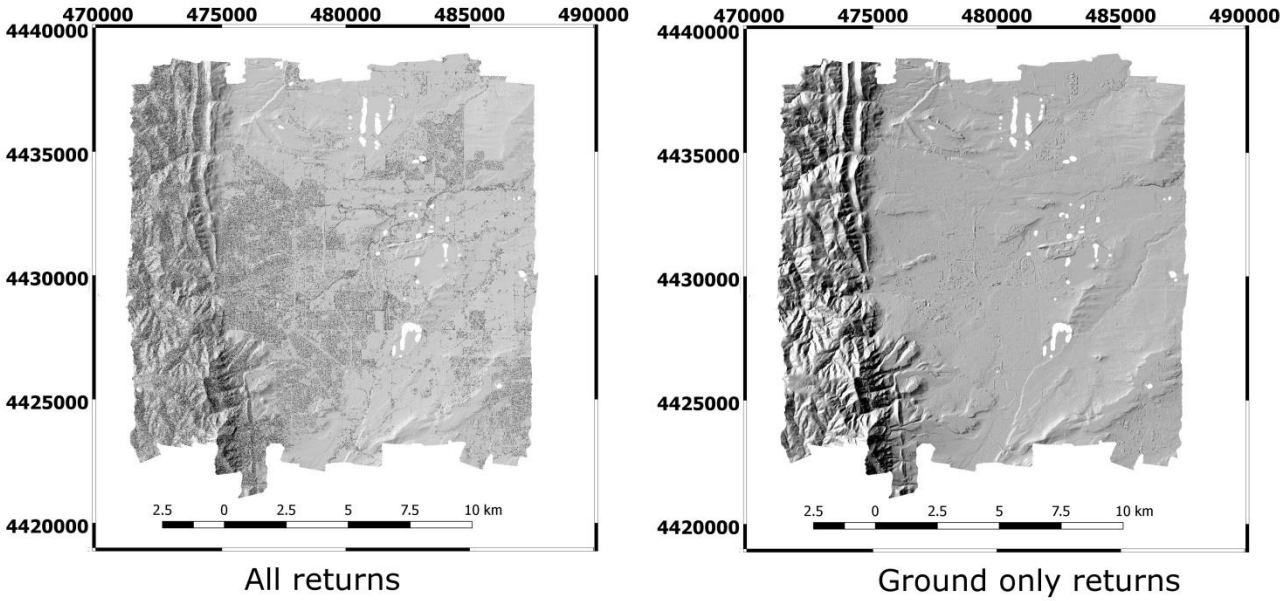

Figure 2 – Comparison of post-flood DTM with all points included (left) and with only the ground returns (right).

3.4 Determination of topographic change

The change map was generated by subtracting the elevation values from the pre-flood DTM and post-flood DTM at each individual grid node location. The DTMs were differenced in the QGIS software package (http://www.qgis.org/en/site/) to provide a grid of the change in elevation between the pre-flood and post-flood acquisitions, which resulted in a DOD (DTM of difference). The pre-flood DTM was subtracted from the post-flood DTM leaving areas which were lower in post-flood dataset as negative values in the DOD and vice versa. Quantitative analysis of the accuracy of the DOD was performed by digitizing profile lines onto 4 paved road surfaces in the DOD. The four roadways selected were Flagstaff Road, Boulder Canyon Road, Sunshine Canyon Road and Highway 36. Flagstaff Road, Boulder Canyon Road, Sunshine Canyon Road were only digitized in the mountainous western portion of the site since interest in the topographic changes will be focused in this area. Highway 36 transits the entire site north to south and nearly transits the east-west extents of the site. Profile lines were created through a manual procedure, leaving the horizontal interval between successive points variable, but at approximately 1 point/m. The profile lines were drawn along paved surfaces which were known to remain relatively unchanged between the pre-flood and post-flood surveys, although some construction was present on Highway 36. Given the

stable road conditions, if the pre-flood and post-flood surveys were error-less the observed change should be zero.

4 RESULTS AND DISCUSSION

4.1 AIRBORNE TRAJECTORY DATA PROCESSING RESULTS

The results of the aircraft trajectory processing showed that all trajectories achieved centimeter level errors for the majority of the acquisition time across each flight day (Figure 2). The highest level of trajectory error for all flights occurred during the post-flood acquisitions, and reached a magnitude of approximately 0.06 m. Note that high levels of error occurring at the beginning or end of each trajectory are due to system initialization and can be ignored, as they did not occur during periods of LIDAR data acquisition. The error levels observed in the trajectories are an important component to understanding the total error in the final results as they dictate the minimum amount of error which will propagate into the change analysis map. For example, *Goulden and Hopkinson* (2010) identify that under conditions of near nadir scan angles and instances of low roll and pitch the trajectory error can account for up 90% of the total error. It should be expected that, at best, the results of the change analysis map will be slightly less accurate than the combined error in the trajectory between the pre-flood and post-flood acquisition for any given observation.

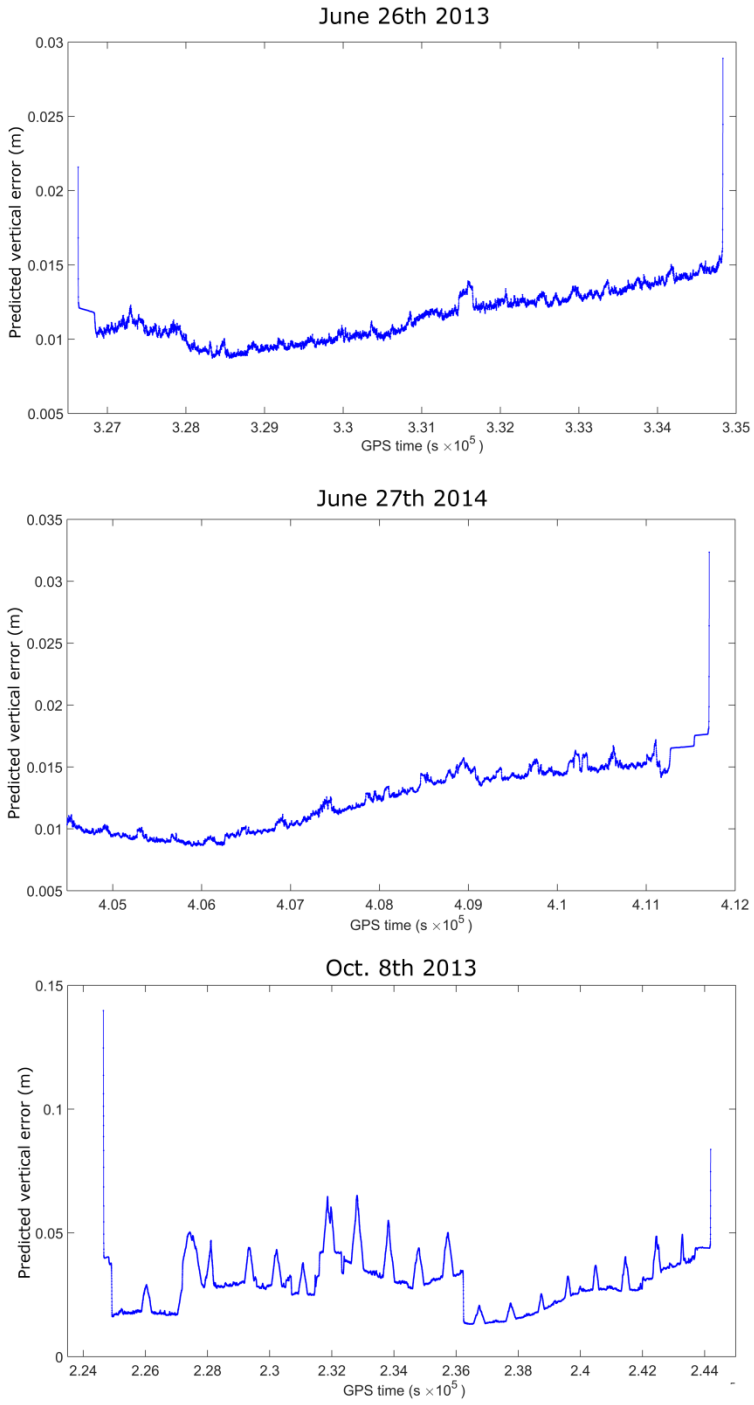

Figure 3 – Predicted vertical errors of the airborne trajectory for each flight day of the pre-flood and post-flood LIDAR acquisitions.

4.2 LIDAR POINT CLOUD PROCESSING RESULTS

Upon processing of the point clouds, the strip to strip matching prior to application of refined processing showed that the majority of relative errors between adjacent strips ranged between -0.25 m to 0.25 m. There was a slight systematic bias in the observations which manifested as a negative increase in point to plane distances at negative scan angles. After the refined processing procedure was applied, the systematic bias has been removed as shown by the random behavior of the point to plane distances with respect to scan angle (Figure 4). Additionally, the overall precision of the data set is reduced after refined processing, with results of all point to plane distances being approximately bounded between ±0.10 m (Figure 4). Users should be cautioned that applying the refined processing method to flight lines from both the pre-flood and post-flood acquisitions simultaneously will potentially degrade the absolute accuracy of the data in order to increase the relative accuracy. Therefore, the pre-flood and post-flood data should only be used to analyze relative differences between the pre-flood and post-flood data sets. If a user is interested in either the pre-flood or post-flood surveys with higher absolute fidelity, but lower relative compatibility, they are encouraged to contact NEON with this request (contact information is supplied in the conclusion of this document).

The refined processing results generally indicate that the resulting precision of the LIDAR sensor measurements is near ±0.10 m; however, results of the refined processing provide only global statistics of the entire dataset. It is known that particular surface conditions will cause increases in error, such as terrain slope or presence of vegetation (*Huising and Gomes Pereira*, 1998; *Hodgson and Bresnahan*, 2004; *Hyyppa et al.,* 2005; *Joerg et al.*, 2012; *Goulden and Hopkinson*, 2014). Landscape with high terrain slope and vegetation exist primarily in the western portion of the survey which comprises less than 10% of the total area. The majority of the survey exists over the urban center, and agricultural lands in the east where the data will tend to have a higher accuracy. Therefore, the global statistics provided by the refined processing may not be representative of the error in the higher sloped western mountainous / vegetative region.

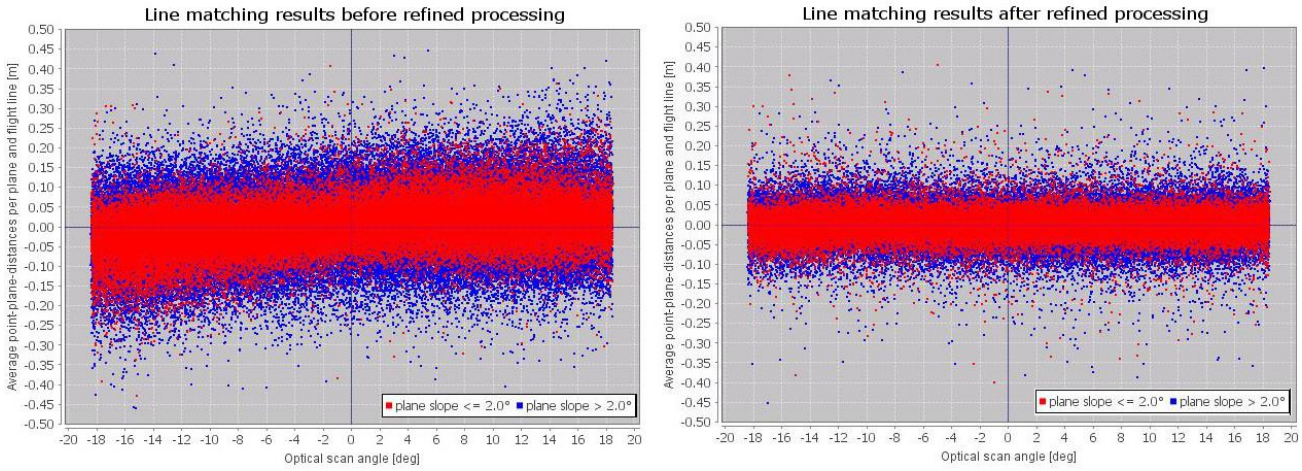

Figure 4 – Mean point to plane distances before and after the application of refined processing

4.3 DTM of Differences (DOD)

The subtraction of the pre-flood and post-flood DTMs yielded a DOD in which 95% of the raster cells showed change which fell between -0.185 and 0.208 m, with a mean of 0.013 m (Figure 5). Given the LIDAR processing results placed the potential errors in the sensor at approximately ±0.1 m; some portion of the DOD results can be confidently considered physical change and not change artifacts due to sensor error. Change results for the four tested roadway profiles, where it can be assumed no change had occurred, can be seen in Table 2. Along the roadway profiles, the mean change errors ranged between -0.01 m and 0.032 m. The low magnitude of change indicates a high level of relative accuracy between the pre-flood and post-flood datasets, providing confidence that observed changes in other regions of the DOD are real. The associated standard deviations of the observed errors on the road surface with a mean trend removed were also minor, ranging from 0.017 to 0.049 m.

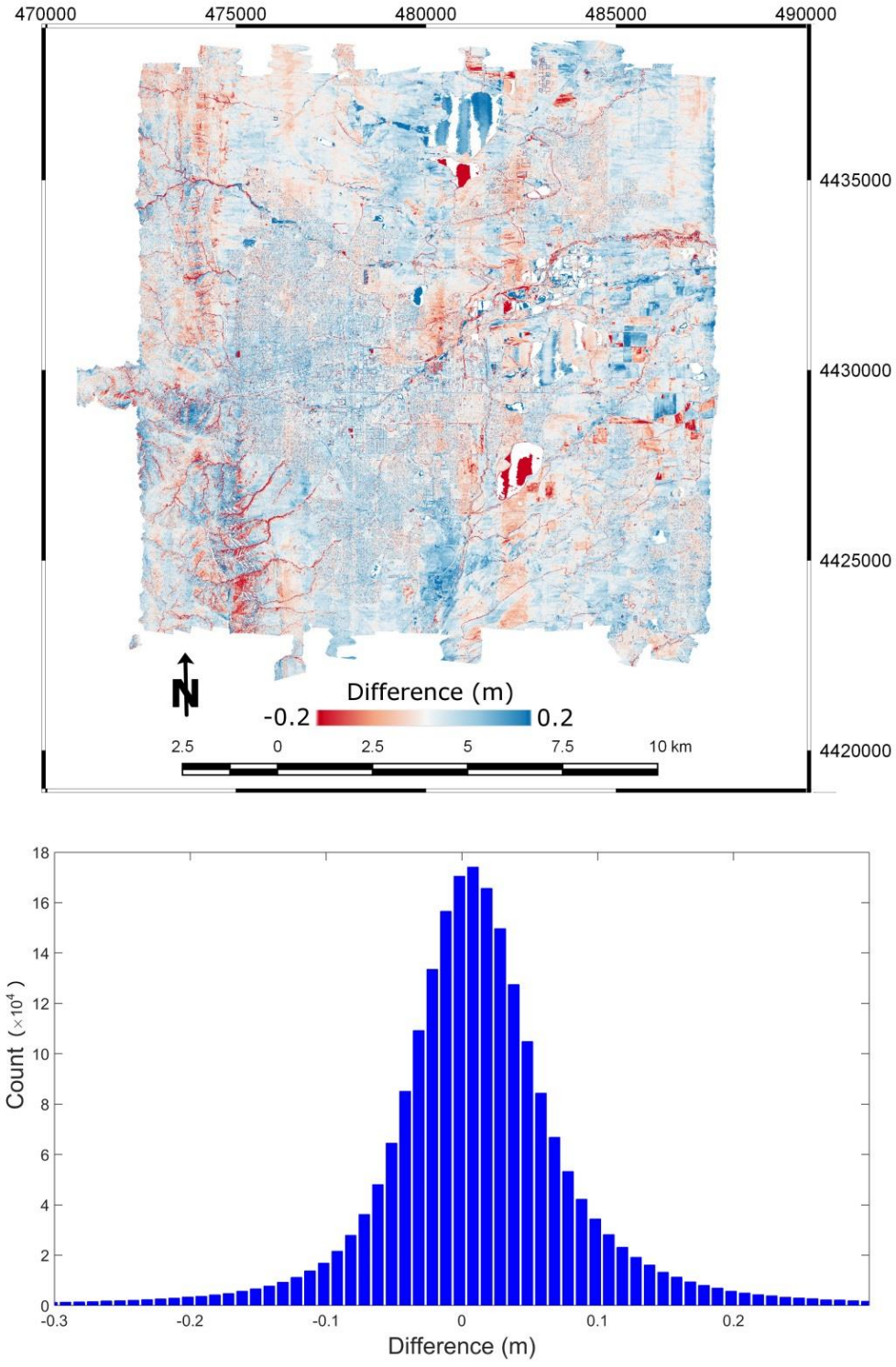

Figure 5 – DOD for the pre-flood and post-flood surveys with associated histogram

The roadway with the largest incidence of change error was collected on Highway 36. The higher incidence of error on Highway 36 can likely be attributed to vehicles present on the roadway which were incorrectly filtered, as well as on-going construction occurring on the highway in both the pre-flood and post-flood surveys which changed the elevation of the road surface. The least amount of error observed on the tested road profiles occurred on Flagstaff road. The error on Flagstaff road profile resulted in a mean of -0.01 m and a standard deviation of 0.026, indicating a very high spatial match between the pre-flood and post-flood datasets. Although results from the roadway show levels of compatibility much higher than the ±0.1 m that resulted from the strip matching results in Section 4.2, it should be noted that the characteristics of roadway surfaces (hard, flat and reflective) provide ideal conditions for collecting accurate LIDAR sensor observations. As previously noted in Section 4.2, LIDAR observational error will tend to increase in the presence of complexities in the landscape such as terrain slope or vegetation. Therefore, the results from the road profiles provide confidence that the relative compatibility of the pre-flood and post-flood DTMs is high; however, the magnitude of differences observed on the roadways cannot necessarily be extrapolated to the remainder of the dataset. For example, given the worst result along a tested road profiles was 0.051 m, it cannot be assumed that this magnitude of error is the worst case scenario across the entire data set and that change which is above this threshold is physical. Areas with large amounts of vegetation or high terrain slope could experience larger errors, which are more difficult to quantify and separate from actual change. A more conservative general estimate of the error is the ±0.1 m result from the strip matching, although this may also be slightly optimistic in areas of high slope or heavy vegetation.

Table 2 – Results of the road profile comparisons

Road	Mean difference (m)	Standard Deviation (m)	Standard Deviation w/ trend removed (m)
Boulder Canyon Road	0.020	0.031	0.023
Sunshine Canyon Drive	0.019	0.036	0.024
Flagstaff Road	-0.010	0.026	0.017
Highway 36	0.032	0.051	0.049

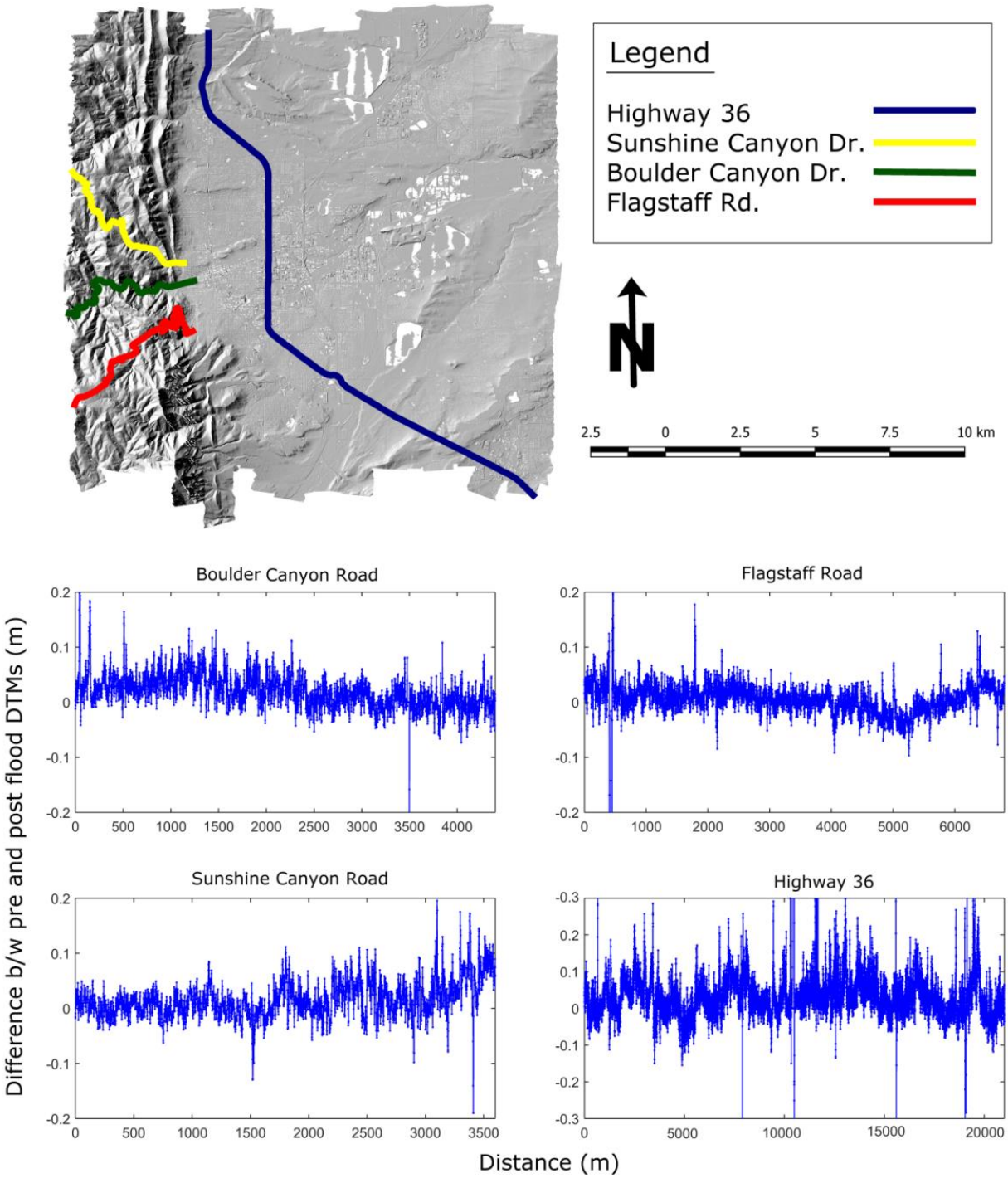

Figure 6 – Results of the road profile analysis in the DOD

In addition to the ±0.1 m of error that identified to be due to sensor error in Section 4.2, there are additional sources of processing uncertainty that were noted in the DOD which can increase the error in the DOD. These sources of uncertainty can be separated into three categories; 1) inaccurate strip matching during refined processing, 2) inaccurate filtering of ground points and 3) interpolation across data gaps. The resulting values in the DOD which result from these artifacts can cause the change error to extend past the ±0.1 m threshold noted in Section 4.2 and therefore cannot be trusted to provide a realistic estimate of the true change. Change artifacts due to category one, inaccurate strip matching, will cause residual vertical errors which manifest as change patterns in the DOD which follow the footprint of a flight swath. For example, a north-south line of change is evident as an approximate easting of 483000 (Figure 5). The profile data for Highway 36 also transits through this section at approximately the 5000 m mark, where there is a section of noticeable decline with magnitude of approximately -0.1 m (Figure 6). Typically, the additional error introduced through inaccurate strip matching will be on the order of centimeters to a decimeter.

Change artifacts from category two result from imperfect classification of ground and non-ground points during filtering. This exists because no filtering algorithm can achieve 100% accuracy, and some points will be incorrectly classified in both the pre-flood and post-flood data sets. For example, it is possible that laser echoes from a building or vegetation were classified as ground in the pre-flood survey but not the post-flood survey. A point incorrectly classified as ground will contribute to the development of the DTM, which is subsequently used in the creation of the DOD. If a vegetation or building return was incorrectly classified as a ground point in the pre-flood results, but not the post-flood results, an artificial change artifact will occur. Such artifacts are most easily identified in the urban areas where the classification routine tends to perform more poorly (*LAStools*, 2014). Change errors introduced through improper filtering can be on the order of centimeters to meters.

Change artifacts from category three can trace back to the decision to interpolate distances under 10 m identified in Section 3.3, in order to create a continuous surface model. Artifacts can appear where interpolation was necessary in either the pre-flood or post-flood DTM, but not the other. This often occurs in areas where a large group of points were defined as ‘non-ground’ during the classification routine, such as within building footprints, and indicates the algorithm determined they were surface features. Non-ground points are not used in DTM creation and the DTM is interpolated across these regions. Interpolated regions will be highly inaccurate which results in change artifacts within the boundary of the interpolated area. Additionally, some areas larger than the 10 m interpolation threshold were determined to be ‘non-ground’, which left gaps in the data. The largest gaps occurred on some sharp peaks in the western

mountainous region of the survey, which were not correctly classified as ground points by the classification routine. The edges of the data gaps tend to be interpolated, which results in a border around data gaps which show highly inaccurate levels of change. Change errors introduced through interpolation filtering can be on the order of centimeters to several meters.

Despite the levels of uncertainty in the DOD, definite patterns of change can still be identified within the survey area. Most noticeable are changes which occurred as a result of stream flow processes, as identifiable sections of substantial deposition (positive change) and erosion (negative change) within stream channel boundaries. Areas of substantial erosion often occurred in the steepest portion of stream channels, or in transitional areas from high sloped areas to low sloped areas. An area south of Lee Hill drive, where the stream course transitioned from a high slope mountain stream to low sloped area was particularly affected (Figure 6). In this region soil loss surrounding the stream bed was in excess of 3 m and downstream deposition reached over 2 m. Outside of stream channels, erosion attributed to overland flow can be identified in some headwater regions of stream channels. These patterns are most identifiable near the south west corner of the site, below Flagstaff road as streams initiate in the mountains, and flow easterly into the urban areas of the City of Boulder. These larger areas of erosion appear to correspond with landslide observations made shortly after the flood event by the Boulder Creek critical zone observatory (http://criticalzone.org/boulder/). Here, erosion levels over large areas (tens of hectares) reached 0.2 to 0.3 meters. Although the overall magnitude of change in these regions was much lower than in the stream channels, the larger areas of erosion potentially leads to higher volumes of soil loss.

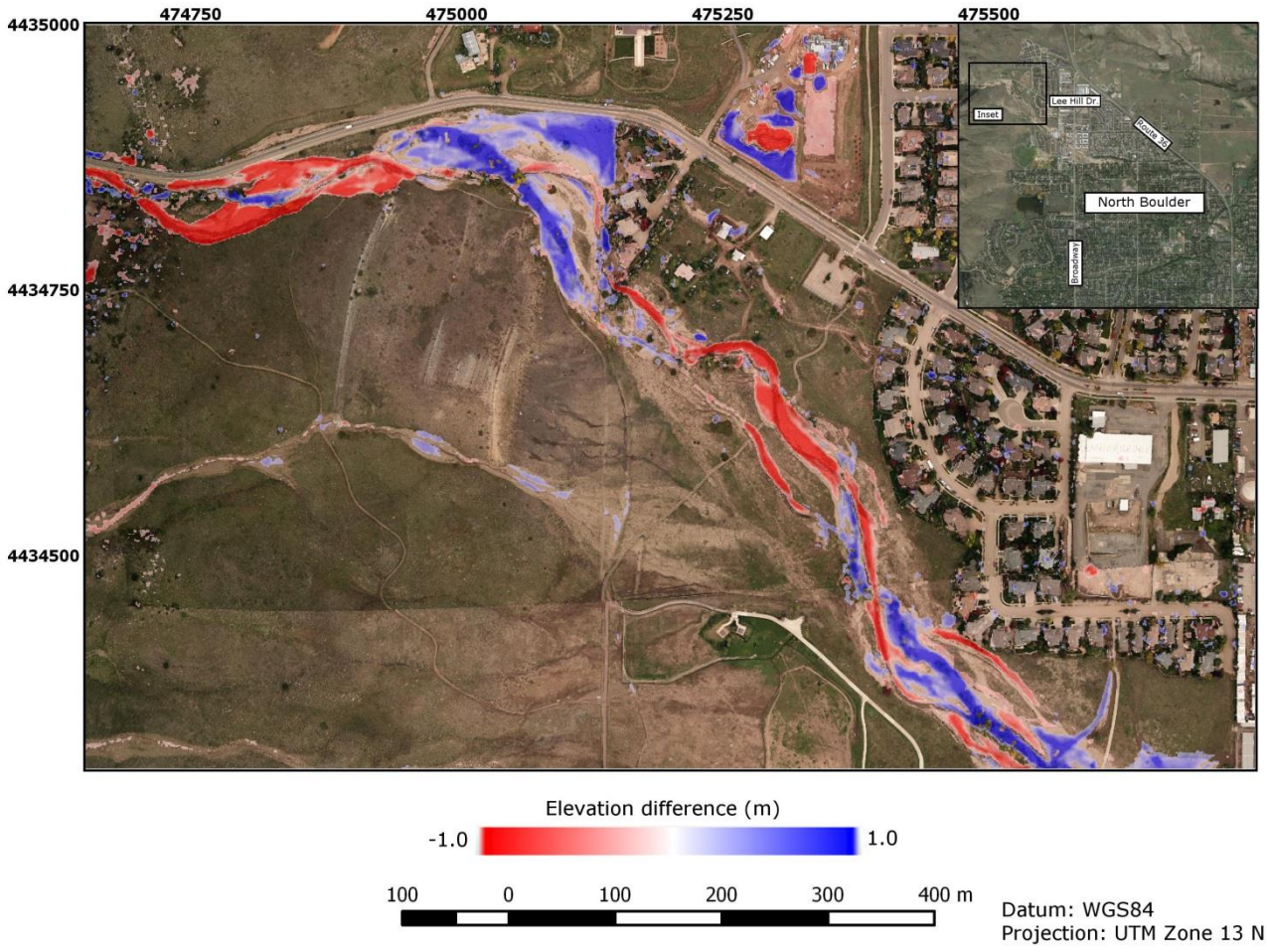

Figure 7 – Topographic changes observed in the stream channel south of Lee Hill Drive

CONCLUSION

The fortuitous timing of a pre-flood LiDAR survey of the city of Boulder by NEON, and a planned post flood LiDAR survey afforded an extraordinary dataset to investigate topographic changes due to the extreme storm event. Change was determined through a DOD, which was a subtraction of grid based DTMs determined from the pre-flood and post-flood acquisitions. Given the error characteristics of the LiDAR sensor and uncertainty introduced in processing, observed changes under ± 0.10 m can likely be considered anomalies and not physical change. Errors above this threshold, unless due to interpolation or improper filtering of non-ground points can generally be considered to be physical change that has resulted from the storm event. Identifiable changes were primarily constrained to stream channels, which often experienced extreme levels of erosion or deposition. Some erosional changes could be noted over larger areas as a result

of overland flow, and which had magnitude of up to ~0.30 m. Although the magnitude of the erosion due to overland flow was lower than in the stream channels, the total volume of sediment is potentially higher due to the larger areas of soil loss.

If readers are interested in obtaining the LIDAR point cloud data used to develop the DOD in the form of LAS 1.3 files, or the DTMs and DOD in geoTIFF format they are encouraged to contact NEON at AOP-Data@neoninc.org with contact information.

ACKNOWLEDGEMENTS

The National Ecological Observatory Network is a project sponsored by the National Science Foundation and managed under cooperative agreement by NEON, Inc. This material is based in part upon work supported by the National Science Foundation. Any opinions, findings, and conclusions or recommendations expressed in this material are those of the authors and do not necessarily reflect the views of the National Science Foundation. This material was supported by the National Science Foundation under Grant DBI-0752017.

REFERENCES

ASPRS, 2010. LAS Specification, Version 1.3 – R11, American Society of Photogrammetry and Remote Sensing, 5410 Grosevenor Lane, Suite 210, Bethesda Maryland

Applanix, 2013. PosPac mobile mapping suite. Applanix, available on-line at http://www.applanix.com/products/airborne/pospac-mms.html, last accessed January 2015.

Axelsson, P. (2000). DEM generation from laser scanner data using adaptive TIN models. *International Archives of Photogrammetry and Remote Sensing*,*33*(B4/1; PART 4), 111-118.

Baltsavias, E. P., 1999. Airborne laser scanning: basic relations and formulas, ISPRS Journal of Photogrammetry and Remote Sensing, 54 (2-3), 199-214. DOI: 10.1016/S0924-2716(99)00015-5

Brennan, C., and J. Aguilar, 2013. Eight days, 1000-year rain, 100 year flood, Daily Camera, available on-line at http://www.dailycamera.com/news/boulder-flood/ci_24148258/boulder-county-colorado-flood-2013-survival-100-rain-100-year-flood, last accessed January 2015.

Goulden, T. and C. Hopkinson, 2010. The forward propagation of integrated system component errors within airborne lidar data. Photogrammetric Engineering and Remote Sensing, 76(5), 589-601

Goulden and Hopkinson, 2014. Mapping simulated error due to terrain slope in airborne lidar observations, International Journal of Remote Sensing, 35(20), 7099-7117

Hodgson, M. E., & Bresnahan, P. (2004). Accuracy of Airborne Lidar-Derived Elevation. *Photogrammetric Engineering & Remote Sensing*, *70*(3), 331-339.

Huising, E. J., & Gomes Pereira, L. M., 1998. Errors and accuracy estimates of laser data acquired by various laser scanning systems for topographic applications. *ISPRS Journal of Photogrammetry and Remote Sensing*, *53*(5), 245-261.

Hyyppä, H., Yu, X., Hyyppä, J., Kaartinen, H., Kaasalainen, S., Honkavaara, E., & Rönnholm, P. (2005). Factors affecting the quality of DTM generation in forested areas. *International Archives of Photogrammetry, Remote Sensing and Spatial Information Sciences*, *36*(3/W19), 85-90.

Joerg, P. C., Morsdorf, F., & Zemp, M. (2012). Uncertainty assessment of multi-temporal airborne laser scanning data: A case study on an Alpine glacier. *Remote Sensing of Environment*, *127*, 118-129.

Kampe, T. U., B. R. Johnson, M. Kuester, and M. Keller, "NEON: the first continental-scale ecological observatory with airborne remote sensing of vegetation canopy biochemistry and structure," J. Appl. Remote Sens., 4, 043510 (2010) [doi:10.1117/1.3361375].

Lindenthal, S.M., V.R. Ussyshkin, J.G. Wang, M. Pokorny, 2011. Airborne LiDAR: A fully automated self-calibration procedure, International archives of the Photogrammetry, Remote Sensing and Spatial Information Sciences, Volume XXXVIII-5/W12, ISPRS Calgary Workshop, 29-21 August 2011, Calgary, Canada.

Lukas, J., 2013. Severe flooding on the Colorado Front Range, CIRES / WWA, available on-line at http://wwa.colorado.edu/resources/front-range-floods/assessment.pdf, last accessed January 2015.

Moore, I.D., Grayson, R.B., Ladson, A.R., 1991. Digital terrain modelling: a review of hydrological, geomorphological, and biological applications. Hydrological Processes, 5(1): 3-30. DOI: 10.1002/hyp.3360050103

NOAA, 2013. Precipitation totals – 7 day totals – Sept 9th through Sept 15th 2013, National weather service, Denver / Boulder, CO weather forecast office, available on-line at http://www.crh.noaa.gov/bou/?n=preciptotals_multiday, last accessed January 2015.

Nuth, C. and A. Kääb, 2012. Co-registration and bias corrections of satellite elevation data sets for quantifying glacier thickness change. The Cryosphere (5), 271-290. DOI: 10.5194/tc-5-271-2011

Optech, 2008. ALTM Gemini, Optech Incorporated, 300 Interchange Way, Vaughn, ON, Canada, available on-line at http://pdf.directindustry.com/pdf/optech/altm-gemini/25132-53143.html, last accessed January 2015.

RapidLasso, 2014. Lasground Readme, RapidLasso (http://rapidlasso.com/), Version 140730

Shan, J., & Toth, C. K. (Eds.). 2008. *Topographic Laser Ranging and Scanning: Principles and Processing*. CRC Press. Vosselman, G. V., & Maas, H. G. (Eds.), 2010. *Airborne and Terrestrial Laser Scanning*. Whittles.

Wehr, A., and U. Lohr, 1999. Airborne laser scanning – an introduction and overview. ISPRS Journal of Photogrammetry and Remote Sensing, 54, 68-82.